

Current helicity and electromotive force of magnetoconvection influenced by helical background fields

G. Rüdiger and M. Küker

Leibniz-Institut für Astrophysik Potsdam, An der Sternwarte 16, D-14482 Potsdam, Germany, email: gruediger@aip.de, mkueker@aip.de

Received; accepted

ABSTRACT

Motivated by the empirical finding that the known hemispheric rules for the current helicity at the solar surface are not strict, the excitation of small-scale current helicity by the influence of a large-scale helical magnetic background fields on nonrotating magnetoconvection is demonstrated. It is shown within a quasilinear analytic theory of driven turbulence and by nonlinear simulations of magnetoconvection that the resulting small-scale current helicity has the same sign as the large-scale current helicity while the ratio of both pseudo-scalars is of the order of the magnetic Reynolds number of the convection. The same models do not provide finite values of the small-scale kinetic helicity. On the other hand, a turbulence-induced electromotive force is produced including the diamagnetic pumping term as well as the eddy diffusivity but no α effect. It is thus argued that the relations by Pouquet & Patterson (1978) and Keinigs (1983) for the simultaneous existence of small-scale current helicity and α effect do not hold for the considered model of nonrotating magnetoconvection. Calculations for various values of the magnetic Prandtl number demonstrate that for the considered diffusivities the current helicity grows for growing magnetic Reynolds number which is not true for the velocity of the diamagnetic pumping – in agreement with the results of the quasilinear analytical approximation.

Key words. Magnetohydrodynamics (MHD) – Magnetic fields – convection – Sun: activity

1. Introduction

An increasing number of observations concerns the small-scale current helicity

$$\mathcal{H}_{\text{curr}} = \langle \mathbf{b}(\mathbf{x}, t) \cdot \text{curl} \mathbf{b}(\mathbf{x}, t) \rangle \quad (1)$$

at the solar surface, all showing that it is negative (positive) in the northern (southern) hemisphere (Hale 1927; Seehafer 1990; Rust & Kumar 1994; Abramenko et al. 1996; Bao & Zhang 1998; Pevtsov 2001; Kleeorin et al. 2003; Zhang et al. 2010; Zhang 2012). Here the notation \mathbf{b} denotes the fluctuating parts of the total magnetic field in the form $\mathbf{B} = \bar{\mathbf{B}} + \mathbf{b}$. It became clear that the scalar quantity (1) shows a strict equatorial antisymmetry with signs which do not change from cycle to cycle. Note that for the linear α^2 dynamo as well as the simple $\alpha\Omega$ dynamos the large-scale helicity $\bar{\mathbf{B}} \cdot \text{curl} \bar{\mathbf{B}}$ similar to (1) also shows equatorial antisymmetry in accordance with $\text{sign}(\bar{\mathbf{B}} \cdot \text{curl} \bar{\mathbf{B}}) = \text{sign}(\alpha)$ (Steenbeck & Krause 1969). That for flux transport $\alpha\Omega$ dynamos the relation is much more complicated (positive correlation only during the cycle minima) indicates that a direct relation $\alpha \propto \bar{\mathbf{B}} \cdot \text{curl} \bar{\mathbf{B}}$ not necessarily exists. It is nevertheless important that all the mentioned scalars such as helicities and α effect are pseudoscalars which might be related to each other.

There are many theoretical studies where both the current helicity and the α effect are derived as consequences of the existence of the pseudoscalar $\mathbf{g} \cdot \boldsymbol{\Omega}$ in rotating convection zones with \mathbf{g} as the (radial) direction of stratification. Yet it is shown in the present paper that the current helicity can also be produced even without rotation if the convection is influenced by a magnetic background field which is helical. Then the question is whether the same constellation would also lead to a turbulence-induced

electromotive force via an α effect as suggested by the relation

$$\alpha = -\eta \frac{\langle \mathbf{b}(\mathbf{x}, t) \cdot \text{curl} \mathbf{b}(\mathbf{x}, t) \rangle}{\bar{\mathbf{B}}^2} \quad (2)$$

of Keinigs (1983). It is based on the existence of homogeneous and stationary turbulence with finite kinetic helicity (Seehafer 1996) which conditions are obviously not fulfilled if one of the magnetic field components is inhomogeneous. Pouquet & Patterson (1978) presented the relation

$$\alpha \propto \frac{1}{\mu_0 \rho} \langle \mathbf{b} \cdot \text{curl} \mathbf{b} \rangle - \langle \mathbf{u} \cdot \text{curl} \mathbf{u} \rangle, \quad (3)$$

which also means that even turbulent fluids with vanishing kinematic helicity but finite small-scale current helicity should possess an α effect but with opposite sign as in (2).

Studies by Yousef et al. (2003), Blackman & Subramanian (2013) and Bhat et al. (2014) concern the dissipation of helical and nonhelical large-scale background fields under the influence of a nonhelical turbulent forcing. It is shown in these papers that the kinematic helicity is dominated by the magnetic helicity which is confirmed by our quasilinear calculations for forced turbulence and the nonlinear simulations of magnetoconvection under the influence of a large-scale helical field. In contradiction to the relation (3) both the quasilinear approximation and nonlinear simulations provide reasonable values for the current helicity but they do not lead to a finite α effect.

2. The current helicity

In order to find the current helicity due to the interaction of a prescribed stochastic velocity $\mathbf{u}(\mathbf{x}, t)$ and a large scale magnetic field $\bar{\mathbf{B}}(\mathbf{x})$ it is sufficient to solve the induction equation

$$\frac{\partial \mathbf{B}}{\partial t} = \text{curl}(\mathbf{u} \times \mathbf{B}) + \eta \Delta \mathbf{B}, \quad (4)$$

where the fluctuating magnetic field may be written as $\mathbf{B} = \bar{\mathbf{B}} + \mathbf{b}$. The influence of field gradients on the mean current helicity (1) at linear order is governed by

$$\frac{\partial b_i}{\partial t} - \eta \Delta b_i = x_p B_{jp} u_{i,j} - u_j B_{ij}, \quad (5)$$

where the prescribed inhomogeneous mean magnetic field $\bar{\mathbf{B}}$ has been introduced in the form $\bar{B}_j = B_{jp} x_p$ with the notation $\bar{B}_{j,p} = B_{jp}$ and with $B_{jj} = 0$. It follows $\bar{\mathbf{B}} \cdot \text{curl} \bar{\mathbf{B}} = \epsilon_{ilk} B_{ij} B_{kl} x_j$ which is here considered to be the only pseudo-scalar in the system.

To solve the equation (5) the use of the inhomogeneous Fourier modes

$$\begin{aligned} u_i(\mathbf{x}, t) &= \iint \hat{u}_i(\mathbf{k}, \omega) e^{i(\mathbf{k}\mathbf{x} - \omega t)} d\mathbf{k} d\omega, \\ b_i(\mathbf{x}, t) &= \iint (\hat{b}_i(\mathbf{k}, \omega) + x_l \hat{b}_{il}(\mathbf{k}, \omega)) e^{i(\mathbf{k}\mathbf{x} - \omega t)} d\mathbf{k} d\omega \end{aligned} \quad (6)$$

is suggestive. It is a standard procedure which yields

$$\hat{b}_i = -\frac{B_{ij} + \frac{2\eta k_l k_m B_{lm} \delta_{ij}}{-i\omega + \eta k^2}}{-i\omega + \eta k^2} \hat{u}_j, \quad \hat{b}_{il} = \frac{ik_j B_{jl}}{-i\omega + \eta k^2} \hat{u}_i \quad (7)$$

(Rüdiger 1975) from which the small-scale current helicity

$$\mathcal{H}_{\text{curr}} = \iint \langle \hat{\mathbf{b}}(\mathbf{k}, \omega) \cdot \text{curl} \hat{\mathbf{b}}(\mathbf{k}', \omega') \rangle e^{i((\mathbf{k} + \mathbf{k}')\mathbf{x} - (\omega + \omega')t)} d\mathbf{k} d\mathbf{k}' d\omega d\omega' \quad (8)$$

can easily be formed. A homogeneous and isotropic turbulence field with the spectral tensor

$$\hat{Q}_{ij}^{(0)}(\mathbf{k}, \omega) = \frac{E(k, \omega)}{16\pi k^2} \left(\delta_{ij} - \frac{k_i k_j}{k^2} \right) \quad (9)$$

may be postulated where the positive spectrum E gives the intensity of the fluctuations. After manipulations one derives from (8) and (9) the final expression

$$\mathcal{H}_{\text{curr}} = \frac{1}{6} \int_0^\infty \int_{-\infty}^\infty \frac{k^2 E(k, \omega)}{\omega^2 + \eta^2 k^4} dk d\omega \bar{\mathbf{B}} \cdot \text{curl} \bar{\mathbf{B}}. \quad (10)$$

The integral in (10) does only exist for the high-conductivity limit $\eta \rightarrow 0$ after multiplication with η so that

$$\mathcal{H}_{\text{curr}} \simeq \frac{\text{Rm}}{3} \bar{\mathbf{B}} \cdot \text{curl} \bar{\mathbf{B}} \quad (11)$$

scales with the magnetic Reynolds number $\text{Rm} = u_{\text{rms}} \ell_{\text{corr}} / \eta$.

Equations (3) and (11) lead to

$$\alpha \propto -\langle \mathbf{u} \cdot \text{curl} \mathbf{u} \rangle + \frac{\text{Rm}}{3\mu_0 \rho} \bar{\mathbf{B}} \cdot \text{curl} \bar{\mathbf{B}} \quad (12)$$

for the α effect for weak magnetic fields (see Blackman & Brandenburg 2002, Brandenburg & Subramanian 2005).

With our approximations (quasilinear equations, forced turbulence, no rotation) the ratio of the two helicities corresponds to the ratio of the both magnetic energies. Equation (11) requires the same sign for the small-scale and the large-scale current helicities. With (2) one finds $\text{sign}(\alpha) = -\text{sign}(\bar{\mathbf{B}} \cdot \text{curl} \bar{\mathbf{B}})$ which contradicts the above mentioned observations that in the simple α^2 dynamos $\text{sign}(\bar{\mathbf{B}} \cdot \text{curl} \bar{\mathbf{B}}) = \text{sign}(\alpha)$. The only solution of this dilemma is that nonrotating convection under the influence of helical large-scale fields may produce small-scale current helicity but it does not generate an α effect.

If calculated under the same analytical assumptions as the current helicity, the kinetic helicity $\langle \mathbf{u} \cdot \text{curl} \mathbf{u} \rangle$ identically vanishes. Blackman & Subramanian (2013) demonstrated that during the turbulence-induced decay of helical large-scale fields the kinetic helicity remains unchanged. In the quasilinear approximation its part due to the background fields is identically zero. MHD turbulence under the influence of a helical large-scale field is thus suspected to generate current helicity but no kinetic helicity. The question is whether on this basis and after the relations (2) and/or (3) also nonlinear simulations of convection in a stratified plasma provide current helicity but no kinetic helicity and no α effect.

In a previous paper we simulated magnetoconvection under the influence of a uniform vertical magnetic field in order to produce finite values of cross helicity (Rüdiger et al. 2012, from now on referred to as paper I). In the present paper the *helical* magnetic background field

$$B_x = \bar{B}_x \frac{z}{H} \quad B_y = \bar{B}_y \quad (13)$$

with uniform values of \bar{B}_x and \bar{B}_y has been applied to probe the possible production of both small-scale kinetic and current helicity. In the computational layer the vertical coordinate z runs from 0 to $2H$ while the convection zone is located in $[H, 2H]$. The value of the electric-current is $J_y = \bar{B}_x / (\mu_0 H)$. It is $\bar{\mathbf{B}} \cdot \text{curl} \bar{\mathbf{B}} \propto \bar{B}_y \bar{B}_x$ by definition.

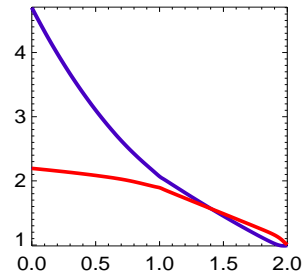


Fig. 1. Snapshots of temperature (red lines) and density (blue lines) during the run for $\bar{B}_x = 10$, $\bar{B}_y = 10$. The surface values are fixed to unity.

The compressible MHD equations have been solved with the NIRVANA code (Ziegler 2004) in a Cartesian box with gravitation along the negative z -axis. The box is periodic in the horizontal directions and all mean-field quantities are averaged over the horizontal plane. For the Prandtl number and the magnetic Prandtl number a common value is fixed to 0.1. As in Paper I the velocities are used in units of $c_{\text{ac}}/100$ where c_{ac} is the speed of sound at the top of the convection box (see Fig. 1). Correspondingly, the magnetic fields are given in units of $\sqrt{\mu_0 \rho} c_{\text{ac}}/100$ with $\mu_0 = 4\pi$. We again assume an ideal, fully ionized gas heated from below and kept at a fixed temperature

at the top of the simulation box. As in paper I the dimensionless Rayleigh number is fixed to 10^7 . Periodic boundary conditions apply at the horizontal boundaries. The upper and lower boundary are perfect conductors so that there for the total magnetic fields

$$\frac{dB_x}{dz} = \frac{dB_y}{dz} = B_z = 0, \quad (14)$$

similar to the stress-free conditions of the velocity, $du_x/dz = du_y/dz = u_z = 0$. At the inner boundary the heat-flux is fixed. One finds in paper I that for very weak magnetic fields the resulting rms-value of the convection velocity in the used units is about 8 (see also the left panel of Fig. 2 below) so that with the dimensionless $\eta = 0.06$ the *global* magnetic Reynolds slightly exceeds 100 which is larger by definition than the local magnetic Reynolds number $Rm = u_{\text{rms}} \ell_{\text{corr}} / \eta$ introduced above.

We start to compute the intensities of the magnetoconvection $u_{\text{rms}}^2 = \langle \mathbf{u}^2 \rangle$ and $b_{\text{rms}}^2 = \langle \mathbf{b}^2 \rangle$ (Fig. 2). The velocity at the top of the convective box results as $\lesssim 10\%$ of the surface value of the sound speed which for the Sun is about 10 km/s. The given time averages and vertical averages in $z=[1,2]$ of all snapshots are taken as the characteristic values of the quantities. The differences of the velocity dispersion to those given in paper I, where much weaker vertical fields have been applied, are very small. The magnetic quenching of the velocity fields does exist but it is weak. However, the ratio $q = \langle \mathbf{b}^2 \rangle / \bar{B}^2$ is strongly affected by the mean magnetic field. While its value is about 30 for the vertical field $B_z = 1$ in paper I the helical field $\bar{B}_x = \bar{B}_y = 10$ only allows q values of order unity. Note also that $u_{\text{rms}}^2 \gtrsim b_{\text{rms}}^2 / 4\pi\rho$, i.e. the convection is *not* magnetic-dominated. Contrary to that, we shall demonstrate that nevertheless the magnetic helicity strongly dominates the kinetic helicity.

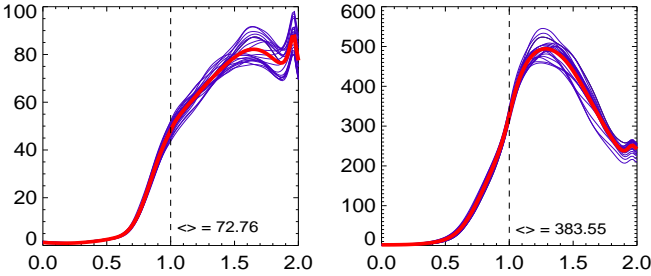


Fig. 2. The turbulence-intensities u_{rms}^2 (left) and b_{rms}^2 (right) for $\bar{B}_x = 10, \bar{B}_y = 10$. The numbers in the graphs are the volume averages of the coefficients over the whole convective domain. The averages over all blue-line snapshots here and in all the below plots are given by solid red lines.

For the same model the correlation coefficients

$$c_{\text{kin}} = \frac{H\langle \mathbf{u} \cdot \text{curl} \mathbf{u} \rangle}{u_{\text{rms}}^2}, \quad c_{\text{curr}} = \frac{H\langle \mathbf{b} \cdot \text{curl} \mathbf{b} \rangle}{b_{\text{rms}}^2} \quad (15)$$

for the kinetic helicity and the current helicity have been computed (Fig. 3). The numerical values strongly differ. While the fluctuations of \mathbf{b} and $\text{curl} \mathbf{b}$ are well correlated this is not true for the flow field.

A systematic behavior of the z -profile does also not exist. In accordance with the analytic quasilinear calculations magnetoconvection subject to helical background fields does not generate

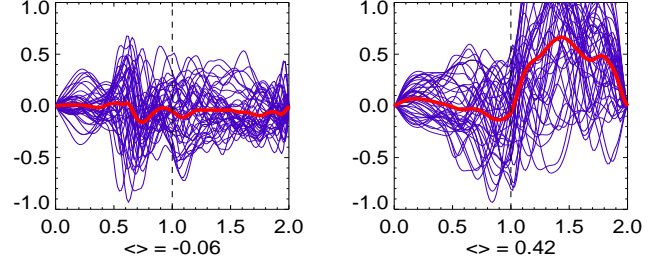


Fig. 3. The same as in Fig. 2 but for the correlation coefficients c_{kin} (left) and c_{curr} (right). The numbers below the graphs are the volume averages of the coefficients over the whole convective domain. The average of all snapshots in both cases is below unity.

small-scale kinetic helicity but it generates small-scale current helicity.

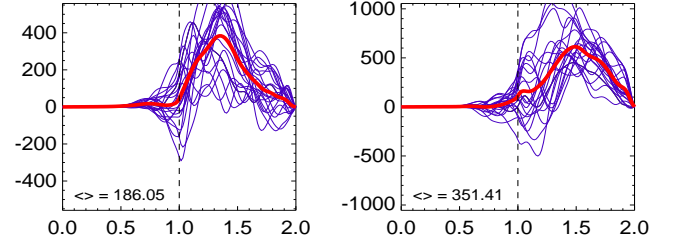


Fig. 4. The small-scale current helicity $\langle \mathbf{b} \cdot \text{curl} \mathbf{b} \rangle$ as due to the large-scale current helicity. Left panel: $\bar{B}_x = 10, \bar{B}_y = 10$, right panel: $\bar{B}_x = 10, \bar{B}_y = 20$. The numbers in the plots mark the averages of all given snapshots. The stratified layer is convectively unstable at the right-hand side of the vertical dashed line where $z > 1$.

The behavior of the magnetoconvection complies with the above analytical result of the incapability of large-scale helical fields to produce small-scale kinetic helicity and they are in correspondence with the numerical result of Bhat et al. (2014) who found the helicities as magnetic-dominated in their simulations of decaying helical background fields under the influence of non-helically driven turbulence.

After (11) one expects for the current helicity numerical values exceeding $\bar{B}_x \bar{B}_y$ which indeed is confirmed by the simulations (Fig. 4). The average number of the right plot is just twice the number in the left plot demonstrating the linear run of the correlations with the the large-scale helicity. The relation (11) which linearly connects the small-scale current helicity with the large-scale current helicity can thus be considered as realized by the numerical simulations. The numerical value between the two helicities and its relation to the magnetic Reynolds number will be discussed below in the section 3.2.

3. The electromotive force

The same magnetoconvection model is used to calculate the turbulence-induced electromotive force. As electric-currents exist in the convection zone it certainly will contain tensorial components of magnetic diffusion. The question is whether also an electromotive force along the magnetic field occurs which must

be interpreted as an α effect. Surprisingly, the answer will be that no α effect is generated by the convection influenced by the helical magnetic background field (15). As simultaneously current helicity without kinetic helicity exists, Eq. (3) cannot be correct for all possible turbulence fields.

The electromotive force $\mathcal{E} = \langle \mathbf{u} \times \mathbf{b} \rangle$ in turbulent plasma is a polar vector. If one wants to express it linearly by the axial mean magnetic field vector $\bar{\mathbf{B}}$ then only the formulation

$$\mathcal{E} = -\eta_T \text{curl} \bar{\mathbf{B}} - \gamma \times \text{curl} \bar{\mathbf{B}} + \dots \quad (16)$$

is possible if pseudoscalars such as $\mathbf{g} \cdot \boldsymbol{\Omega}$ or $\bar{\mathbf{B}} \cdot \text{curl} \bar{\mathbf{B}}$ are not available. Without global rotation an α effect in the formulation $\mathcal{E} = \alpha \bar{\mathbf{B}} \dots$ does not occur in the linear relation (16). The parameter η_T describes the turbulence-induced eddy diffusivity in the fluid while the vector γ gives a velocity which transports ('pumps') the large-scale magnetic field downward for positive γ_z . If, however, terms nonlinear in $\bar{\mathbf{B}}$ are included in the heuristic expression (16) then the extra terms

$$\mathcal{E} = \dots + \hat{\eta} \left(\bar{\mathbf{B}}^2 \text{curl} \bar{\mathbf{B}} + \frac{1}{3} \left[\nabla \bar{\mathbf{B}}^2 + (\bar{\mathbf{B}} \cdot \nabla) \bar{\mathbf{B}} \right] \times \bar{\mathbf{B}} \right) \quad (17)$$

occur within the second-order-correlation approximation (Kitchatinov et al. 1994). The first term of the RHS represents the known magnetic influence on the eddy diffusivity while the second one forms a magnetic-induced pumping effect. There is no term $(\bar{\mathbf{B}} \cdot \text{curl} \bar{\mathbf{B}}) \bar{\mathbf{B}}$ representing an α effect with the large-scale current helicity $\bar{\mathbf{B}} \cdot \text{curl} \bar{\mathbf{B}}$ of the background field as (pseudoscalar) coefficient. For nonrotating and non-helicity driven turbulence the large-scale current helicity does not create an α effect in this approximation. Indeed, we do not find an α effect in the numerical simulations below. There is instead the – sometimes ignored – magnetic-induced new pumping term which for positive $\hat{\eta}$ advects the magnetic field towards the maximum magnetic field. This effect should appear in all numerical models with helical large-scale field and nonhelically driven flow (Yousef et al. 2003; Bhat et al. 2014).

Equations (16) and (17) yield

$$\mathcal{E} = -\left(\eta_T - \hat{\eta} \frac{\bar{\mathbf{B}}^2}{\mu_0 \rho}\right) \text{curl} \bar{\mathbf{B}} - \left(\gamma - \frac{\hat{\eta}}{3} \frac{\nabla \bar{\mathbf{B}}^2}{\mu_0 \rho}\right) \times \bar{\mathbf{B}}. \quad (18)$$

The nonlinear terms magnetically affect both the eddy diffusivity and the advection velocity which are basically reduced if the factor

$$\hat{\eta} = \frac{1}{5} \int_0^\infty \int_{-\infty}^\infty \frac{\eta k^4 (\nu \eta k^4 - \omega^2) E(k, \omega) dk d\omega}{(\omega^2 + \eta^2 k^4)^2 (\omega^2 + \nu^2 k^4)} \quad (19)$$

is positive. The $\hat{\eta}$ possesses the dimension of a time and can be estimated as $\hat{\eta} \simeq \text{Rm}^2 \tau_{\text{corr}}$ in the high-conductivity limit. One easily finds $\hat{\eta} > 0$ for important cases. For $\nu = \eta$ the coefficient $\hat{\eta}$ is always positive for all spectral functions which do not grow with growing frequency. Moreover, for all Pm the full expression (19) is positive for $E \propto \delta(\omega)$ representing long correlation times as well as for $E \simeq \text{const}$, i.e. very short correlation times ('white noise'). If compared with the magnetic-diffusion time $\mu_0 \sigma l_{\text{corr}}^2$ the delta-like spectral line represents the low-conductivity limit while the white-noise spectrum represents the high-conductivity limit. In both limits the $\hat{\eta}$ is positive and, therefore, both eddy diffusivity and diamagnetic pumping are magnetically quenched rather than amplified ('anti-quenched').

3.1. Numerical simulations

The two horizontal components of the electromotive force are calculated for two different cases. In the first simulations the applied magnetic fields are assumed as free of helicity, i.e. $\bar{\mathbf{B}} \cdot \text{curl} \bar{\mathbf{B}} = 0$. The other possibility works with $\bar{\mathbf{B}} \cdot \text{curl} \bar{\mathbf{B}} \neq 0$. If the results of both setups are identical then the global helicity does not contribute to the electromotive force as is suggested by Eq. (17).

Consider first the two different helicity-free cases where in the y direction either only a field or only an electric-current exists. Hence, for $\bar{B}_x = 0$

$$\mathcal{E}_x = \gamma_z \bar{B}_y, \quad \mathcal{E}_y = 0. \quad (20)$$

Figure 5 (left) displays the resulting γ_z as positive (i.e. the flow is downwards) and of order $\gamma_z \simeq 0.24$ in units of $c_{\text{ac}}/100$ which with $c_{\text{ac}} \simeq 10$ km/s approximately¹ leads to a downward pumping of 20 m/s. The simulated electromotive force \mathcal{E}_y vanishes as required by (20).

The alternative example with $\bar{B}_y = 0$ yields $\mathcal{E}_x = 0$ and

$$\mathcal{E}_y = -\left(\left(\eta_T - \hat{\eta} \frac{\bar{B}_x^2}{\mu_0 \rho}\right) + \left(\gamma_z - \frac{2}{3} \frac{z}{H^2} \hat{\eta} \frac{\bar{B}_x^2}{\mu_0 \rho}\right) z\right) \frac{\bar{B}_x}{H}. \quad (21)$$

Indeed, the numerically simulated \mathcal{E}_x vanishes while \mathcal{E}_y is negative (see Fig. 5, right).

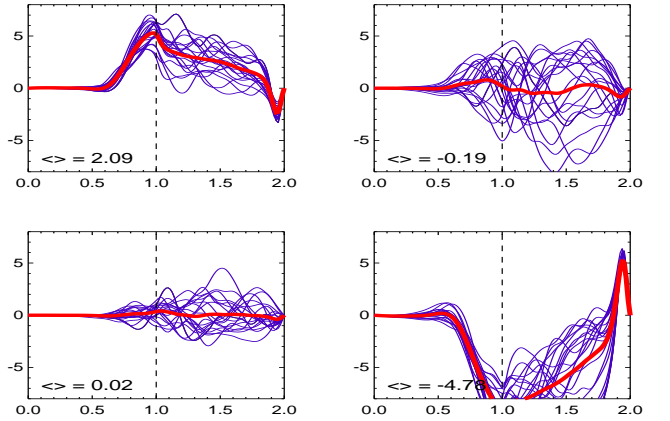


Fig. 5. The two horizontal components (top: \mathcal{E}_x , bottom: \mathcal{E}_y) of the turbulence-induced EMF for background fields without helicity. Left panel: $\bar{B}_x = 0$, $\bar{B}_y = 5$ (only homogeneous magnetic field in y direction); right panel: $\bar{B}_x = 10$, $\bar{B}_y = 0$ (only homogeneous electric-current in y direction). The averages over all snapshots are noted in the plots.

In Fig. 6 the two components of the electromotive force are shown for a field with global helicity, i.e. $\bar{B}_x \bar{B}_y > 0$. From (18) one finds

$$\tilde{\gamma}_z = \frac{\mathcal{E}_x}{\bar{B}_y}, \quad \tilde{\eta} = -H \left(\frac{\mathcal{E}_y}{\bar{B}_x} + \frac{\mathcal{E}_x}{\bar{B}_y} \frac{z}{H} \right), \quad (22)$$

where the tildes mark the magnetically quenched values of the pumping velocity and the eddy diffusivity. The top panels of the

¹ Numerical values in physical units are always given for the top of the unstable zone.

plots only concern the advection velocity $\tilde{\gamma}_z$ which is always positive. It sinks from $\gamma_z \simeq 0.42$ to $\tilde{\gamma}_z \simeq 0.25$ for $B_x = 10$ by the magnetic suppression. From the definition of $\tilde{\gamma}_z$ one immediately finds $\hat{\eta} \simeq 0.02$ for the quenching coefficient (19) in units of $100H/c_{ac}$. The code works with $\rho_0 = 1$.

Note that in all cases the numerical values of $\langle \mathbf{u} \times \mathbf{b} \rangle$ are very small compared with the scalar product u_{rms} and b_{rms} given in Fig. 2. The resulting correlation coefficients are here very small.

The existence of an α effect in the expression (17) for the electromotive force would require a term $(\bar{\mathbf{B}} \cdot \text{curl } \bar{\mathbf{B}})\bar{\mathbf{B}}$. No such term resulted from the quasilinear approximation for the influence of helical large-scale fields on nonhelically driven turbulence. This finding can be probed with the numerical simulations. Note that three models in Figs. 5 and 6 are computed for constant B_x and for growing helicity ($\bar{B}_x \bar{B}_y = 0, 50, 100$). If an α effect existed one should find that the values of \mathcal{E}_y grow for growing helicity. The numerical results for the three models, however, are always identical. They do not show any numerical response to the growing helicities indicating the nonexistence of an α term proportional to $\bar{\mathbf{B}} \cdot \text{curl } \bar{\mathbf{B}}$. The nonexistence of the α term $(\bar{\mathbf{B}} \cdot \text{curl } \bar{\mathbf{B}})\bar{\mathbf{B}}$ in the electromotive force (17) in the quasilinear theory is thus confirmed by nonlinear simulations.

Equation (22) allows to derive the magnetic diffusivity from the simulations. One finds by elimination of $\hat{\eta}$ from the definitions the relation $\eta_T = \tilde{\eta} + (\gamma_z - \tilde{\gamma})H$. With the given mean values for all snapshots the model with $\bar{B}_y = 5$ provides $\tilde{\eta} \simeq 0.11$, so that $\eta_T = 0.27$ in units of $Hc_{ac}/100$ for the unquenched eddy diffusivity. If this result is compared with the traditional estimate $\eta_T \simeq (1/3)u_{\text{rms}}\ell_{\text{corr}}$ one finds $\ell_{\text{corr}}/H \simeq 0.1$. On the other hand, if $\tilde{\eta} = 0$ is used as the definition of a critical magnetic field, i.e. $B_{\text{eq}} = \sqrt{\eta_T/\tilde{\eta}}$, then $B_{\text{eq}} \simeq 3.6$ in units of $\sqrt{4\pi\rho c_{ac}/100}$ so that with $\rho \simeq 10^{-2}$ g/cm³ and $c_{ac} = 10$ km/s the field amplitude $B_{\text{eq}} \simeq 13$ kGauss results in physical units.

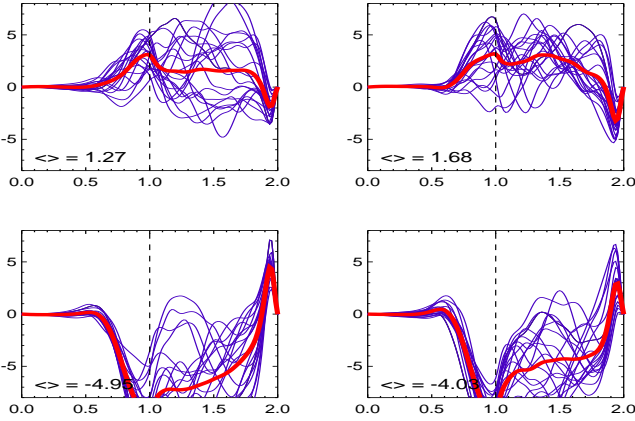


Fig. 6. The same as in Fig. 5 but for the helical background fields with $\bar{B}_x = 10, \bar{B}_y = 5$ (left panel) and $\bar{B}_x = 10, \bar{B}_y = 10$ (right panel). The averages over all snapshots are noted in the plots.

3.2. Variation of the magnetic Prandtl number

It remains to probe the analytical formulation (11) after which the ratio of the small-scale current helicity and the large-scale helicity grows with the magnetic Reynolds number. This is cer-

tainly only true for large values of Rm (high-conductivity limit). Large Rm require high values of the Reynolds number Re and/or not too small Pm . It would certainly be more realistic to increase the Reynolds number rather than the magnetic Prandtl number but our value Re of order 10^3 is the upper limit defined by technical restrictions.

Sofar the simulations have been done with a fixed magnetic Prandtl number $Pm = 0.1$. For fixed molecular viscosity its increase (decrease) by one order of magnitude effectively increases (decreases) the magnetic Reynolds number by a factor of ten. We expect a similar reaction of the small-scale current helicity (11). The reason is that after (11) it grows for growing magnetic Reynolds numbers. Because of $Rm = Pm Re$ for fixed Reynolds number the magnetic Reynolds number runs with Pm .

The results of the variation of the magnetic Prandtl number are shown by the plots given in Fig. 7. From left to right the magnetic Reynolds number sinks by a factor of 33 while the current helicity sinks by a factor of about 17 (i.e. 50% of 33). The current helicity indeed proves to be proportionate to Rm which, however, proves to be smaller than the global magnetic Reynolds number of order 100. Since in paper I for much weaker fields the resulting Rm were much higher the suggestion may be allowed that for the present models the magnetic quenching effect is reducing the numerical values.

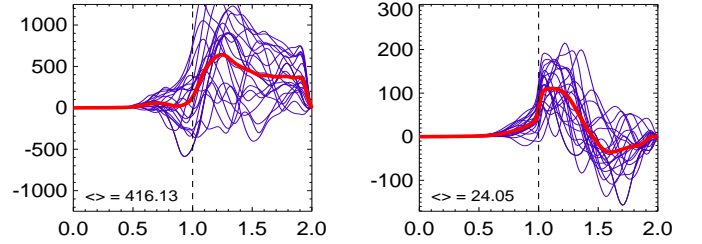


Fig. 7. $\mathcal{H}_{\text{curr}}$ for $\bar{B}_x = \bar{B}_y = 10$. Left panel: $Pm = 1$, right panel: $Pm = 0.03$.

It is easy to give the strength of this statement a test. It is known that the advection term γ_z represented after (20) by \mathcal{E}_x/\bar{B}_y does not vary with Rm (see Kitchatinov et al. 1994). Hence, we do *not* expect a similar behavior as in Fig. 7 for the electromotive force \mathcal{E}_x . Figure 8 indeed shows that for small Rm the reduction of the magnetic Prandtl number by a factor of 33 leaves the electromotive force \mathcal{E}_x basically unchanged.

The results of Figs. 7 and 8 can also be understood as probing the inner consistency of the models and the numerical procedures. It is additionally shown that basic results of the quasilinear approximation are confirmed by simulations.

4. Conclusions

By analytical (quasilinear) theory and numerical simulations it is shown that in a nonrotating convective layer a large-scale helical magnetic background field produces a small-scale current helicity while the kinetic helicity vanishes. The current helicity possesses the same sign as the helicity of the large-scale field. The ratio of both pseudoscalars runs with the magnetic Reynolds number of the convection. The same magnetic model provides

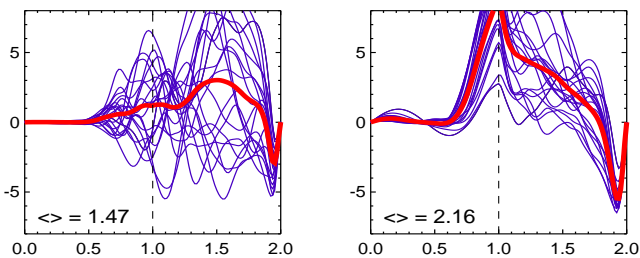


Fig. 8. The same as in Fig. 7 but for \mathcal{E}_x .

finite values of the diamagnetic pumping term γ and the eddy diffusivity η_T but an α effect does not occur in the same order.

If it is true that the α effect in the stellar convection zones is due to the action of the Coriolis force on the turbulent convection then it is positive (negative) on the northern (southern) hemisphere which after Eq. (2) would lead to the opposite signs for the small-scale current helicity – as is indeed observed as dominating during the activity cycle. The new effect of the small-scale current helicity due to the influence of a large-scale field combined with a parallel electric-current yields opposite signs. During the minimum phase of the solar activity cycle just these signs sometimes occur. Zhang et al. (2010) give the approximate value $10^{-5} \text{G}^2/\text{cm}$ for the observed small-scale current helicity. With the radial scale of 100 Mm and with $\bar{B}_r \bar{B}_\phi \simeq 10^4 \text{G}^2$ one only needs a magnetic Reynolds number Rm of the fluctuations of order 10 to fulfill the numerical constraints.

References

- Abramenko, V.I., Wang, T., & Yurichishin, V.B. 1996, *Sol. Phys.*, 168, 75
 Bao, S., & Zhang, H. 1998, *Astrophys. J.*, 496, L43
 Bhat, P., Blackman, E.G., & Subramanian, K. 2014, *MNRAS*, 438, 2954
 Blackman, E.G., & Brandenburg, A. 2002, *Astrophys. J.*, 579, 359
 Blackman, E.G., & Subramanian, K. 2013, *MNRAS*, 429, 1398
 Brandenburg, A., & Subramanian, K. 2005, *Phys. Reports*, 417, 1
 Bräuer, H.J., & Krause, F. 1974, *Astron. Nachr.*, 295, 223
 Hale, G.E. 1927, *Nature*, 119, 708
 Keinigs, R.K. 1983, *Phys. Fluids*, 76, 2558
 Kitchatinov, L.L., Pipin, V.V., & Rüdiger, G. 1994, *Astron. Nachr.*, 315, 157
 Kleorin, N., Kuzanyan, K., Moss, D., et al. 2003, *Astron. Astrophys.* 409, 1097
 Küker, M., & Rüdiger, G. 2016, in prep.
 Pevtsov, A.A., Canfield, R.C., & Latushko, S.M. 2001, *Astrophys. J.*, 549, L261
 Pouquet, A., & Patterson, G.S. 1978, *JFM*, 85, 305
 Rust, D.M., & Kumar, A. 1994, *Sol. Phys.*, 155, 69
 Rüdiger, G. 1975, *Astron. Nachr.*, 296, 133
 Rüdiger, G., & Kitchatinov, L.L. 1997, *Astron. Nachr.*, 318, 273
 Rüdiger, G., Küker, M., & Schnerr, R.S. 2012, *Astron. Astrophys.*, 546, A23
 Rüdiger, G., Kitchatinov, L.L., & Hollerbach, R. 2013, *Magnetic processes in astrophysics: theory, simulations, experiments*. Wiley-VCH Weinheim
 Seehafer, N. 1990, *Sol. Phys.*, 125, 219
 Seehafer, N., *Phys. Rev. E*, 53, 1283 1996
 Steenbeck, M., & Krause, F. 1969, *Astron. Nachr.*, 291, 271
 Yousef, T., Brandenburg, A., & Rüdiger, G. 2003, *Astron. Astrophys.*, 411, 321
 Zhang, H., Sakurai, T., Pevtsov, A., et al. 2010, *MNRAS*, 402, 30
 Zhang, H. 2012, *MNRAS*, 419, 799
 Ziegler, U. 2004, *Comp. Phys. Commun.*, 157, 207